The Predominance of Hydrogen Evolution on Transition Metal Sulfides and Phosphides under CO₂ Reduction Conditions: An Experimental and Theoretical Study

Alan T. Landers,[a, b, 1] Meredith Fields,[b, c, 1] Daniel A. Torelli,[d, 1] Jianping Xiao,[b, c] Thomas R. Hellstern,[b, c] Sonja A. Francis,[d] Charlie Tsai,[b, c] Jakob Kibsgaard,[b, c, e] Nathan S. Lewis,[d, 2] Karen Chan,[b, c, 2] Christopher Hahn,[b, c, 2] Thomas F. Jaramillo[b, c, 2]

a. Department of Chemistry, Stanford University, Stanford, CA 94305
b. SUNCAT Center for Interface Science and Catalysis, SLAC National Accelerator Laboratory, Menlo Park, CA 94025
c. Department of Chemical Engineering, Stanford University, Stanford, CA 94305
d. Division of Chemistry and Chemical Engineering, California Institute of Technology, Pasadena, CA 91125
e. Department of Physics, Technical University of Denmark, DK-2800 Kongens Lyngby, Denmark

1. A.T.L, M.F., and D.A.T. contributed equally to this work.
2. To whom correspondence should be addressed: N.S.L. nslewis@caltech.edu, K.C. chank@stanford.edu, C.H. chahn@slac.stanford.edu, T.F.J. jaramillo@stanford.edu

Supporting Information

Experimental Methods

The molybdenum sulfide and TM phosphide thin films were synthesized using previously reported methods.[1-2] First, ten nanometers of the TM were deposited onto a silicon substrate using electron beam physical vapor deposition. For the TM-doped molybdenum samples, the films were deposited with a Mo:TM ratio of 3:1. Subsequently, a vapor-assisted process in a tube furnace converts the metal thin films into the corresponding TM sulfide or phosphide. The molybdenum thin films convert to the sulfide when heated to 250 ^{o}C under a mixture of H_2 and H_2S gas (*Caution:* H_2S is a highly toxic gas. Both H_2S and H_2 are flammable gases). To convert the samples to phosphides, the metal thin films and a sample of red phosphorus were heated in a tube furnace while flowing H_2 gas (*Caution:* Red phosphorus is a highly flammable solid with an auto-ignition temperature as low as 260 ^{o}C. H_2 is a flammable gas).[1] X-ray photoelectron spectroscopy confirmed the formation of the ionic materials based on the presence of a phosphide peak in the P 2p region, a sulfide peak in the S 2p region, and appropriate metal oxidation states which were consistent with previous reports.[1-2] The materials were evaluated for CO_2R activity in CO_2 sparged 0.10 M $KHCO_3$ using a previously described flow cell.[3] The synthesis for nanoparticulate catalysts is reported elsewhere.[4-6] Briefly, tri-*n*-octyphosphine (TOP) was added as a phosphorus source in equal volume to a 1:1 mixture of 1-octadecene and oleylamine. This mixture was heated to 120 °C under vacuum for 1 hour in a three-necked round-bottom flask equipped with a reflux condenser. The mixture was then heated to 330 °C under Ar and premade metallic nanoparticles suspended in degassed TOP were added and solution was stirred for 1 hr. The resulting solution was then cooled to room temperature, centrifuged and washed with a mixture of hexanes and isopropanol. The resulting nanoparticles were then suspended in hexanes under N_2. To prepare a working

electrode, this suspension was drop cast onto a pyrolytic graphite plate at a loading of 1 mg/cm^2.

The electrodes were then annealed under 5% H_2/N_2 at 400 °C for 1 hr. Thin films of SnS were

synthesized using literature procedures.[7-8] Briefly, bulk SnS powder was dissolved in 11:1 vol/vol

mixture of ethylenediamine and 1,2-ethanedithiol at 50 °C for 15 h at a concentration of 60 mg

mL^{-1}. Solutions were then filtered using a 0.45 µm filter and spin coated onto FTO substrates.

Samples were then annealed on a hot plate at 350 °C under flowing N_2 and finally at 500 °C in a

tube furnace with flowing N_2 to increase robustness for electrochemical measurements.[7-8]

Computational Methods

We have employed QUANTUM ESPRESSO code for total energy calculations, with

plane-wave and density cutoffs of 500 and 5000 eV, respectively. K-point sampling grids of ($2 \times$

2×1) for sulfide surfaces and (4 x 4 x 1) for phosphide surfaces as well as a 0.1 eV Fermi-level

smearing were chosen based on convergence tests from previous work. All calculations

implemented the Bayesian error estimation Functional with Van der Waals correction (BEEF-

vdW) exchange correlation functional. All structures were relaxed until all force components were

< 0.05 eV Å^{-1}. In addition, spin-polarized calculations were performed for all systems containing

Ni, Fe, and Co. For sulfide surfaces, a monolayer of water and explicit H_3O^+ were used to

determine electrochemical transition state for CO protonation to CHO. Barriers were determined

using the climbing image nudged elastic band (NEB) method,[9] and a charge extrapolation

method[10-11] was used to determine the potential dependence of the electrochemical barriers. As

detailed by Chan and Nørskov,[11] a Bader analysis[12] was applied to determine the degree of charge

transfer across the electrochemical interface at the transition states, which provides the

corresponding transfer coefficients. For further calculation details, lattice constants, and

optimization parameters for both phosphides and sulfide surfaces, see corresponding references.[13-15]
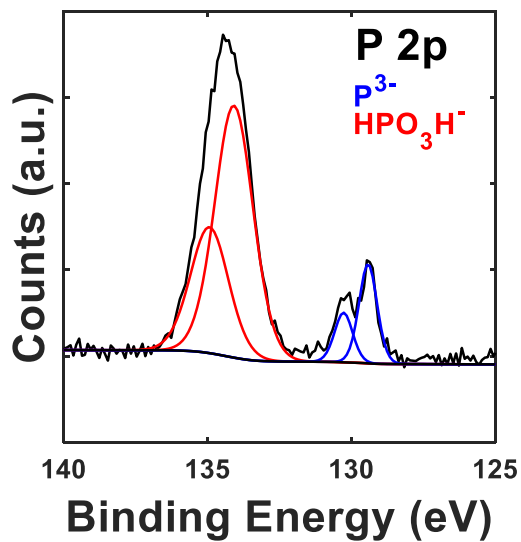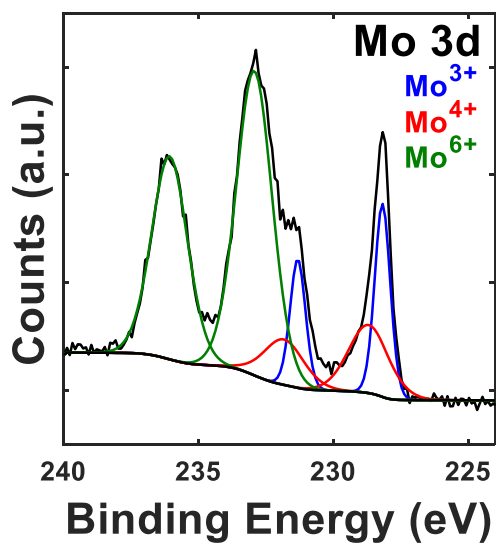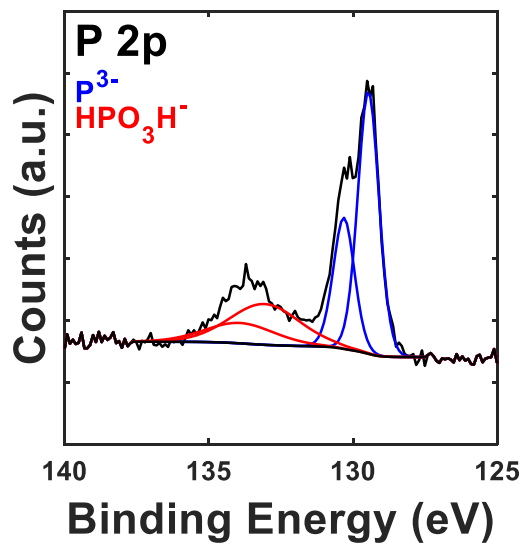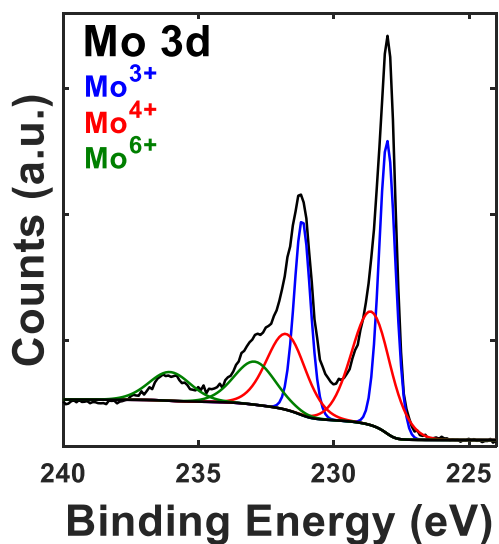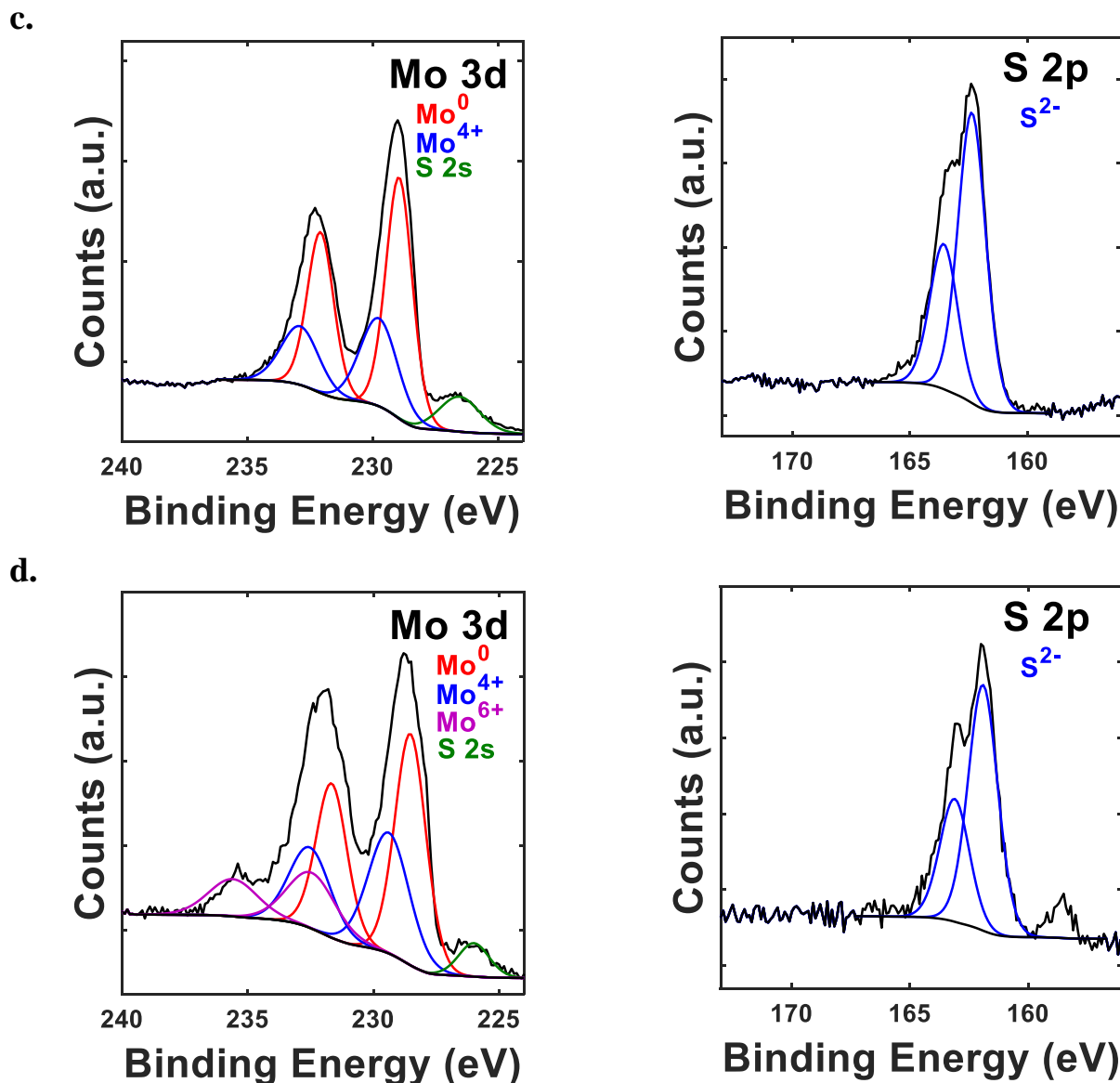
Figure S1. X-ray photoelectron spectra of MoP prior to (**a**) and after (**b**) electrochemical testing. Peaks attributed to Mo^{3+} and P^{3-} are identified.[1] X-ray photoelectron spectra of MoS_2 prior to (**c**) and after (**d**) electrochemical testing. Peaks corresponding to Mo^{4+} and S^{2-} are identified.[2] Note that neither the pre- nor the post-reaction characterization necessarily reflect the surface under electrochemical conditions. Oxidized species at the surface could be reduced at the negative potentials applied during electrolysis. After the electrolysis finishes, the sample briefly returns to its open circuit value in the electrolyte before being removed to the atmosphere and transferred to

the XPS. During this transfer process, the surface of the material could become oxidized relative to its state under electrochemical conditions. To understand the actual surface during CO_2R conditions, in situ characterization would be required.
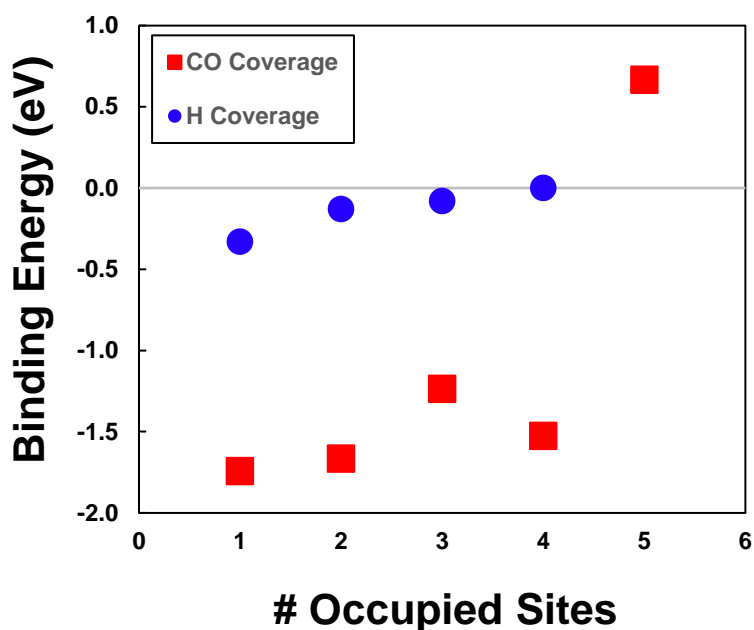
Figure S2: CO preferentially adsorbs on the metal sites of the CoP surface. While the *CO

binding energy decreases slightly with increasing *CO coverage, it is only when all Co metal

sites are saturated and the *CO is forced to occupy a P-site that the binding energy weakens

substantially. It is possible that at steady state, the CoP surface is operating at higher coverages

of *CO than addressed in the DFT thermodynamic analysis. Full kinetic analysis would be

required to determine true steady state coverages.

a.

Decreased Electron Density

Increased Electron Density

b.

Decreased Electron Density

Increased Electron Density
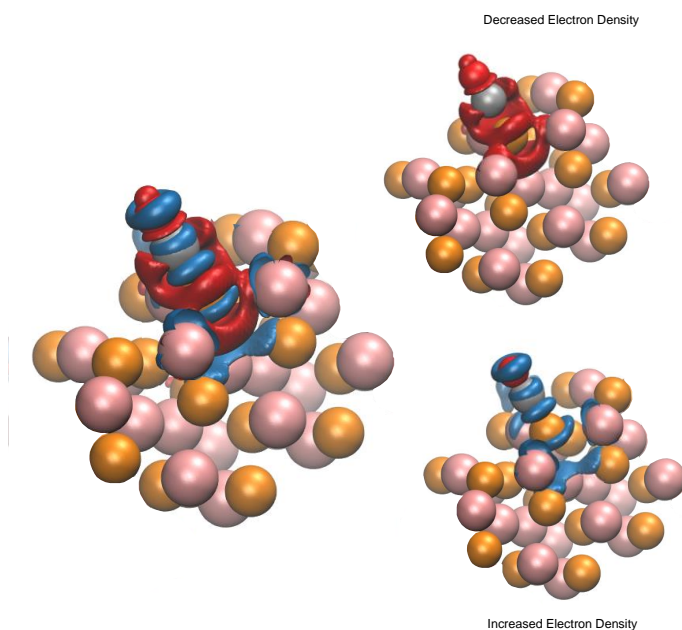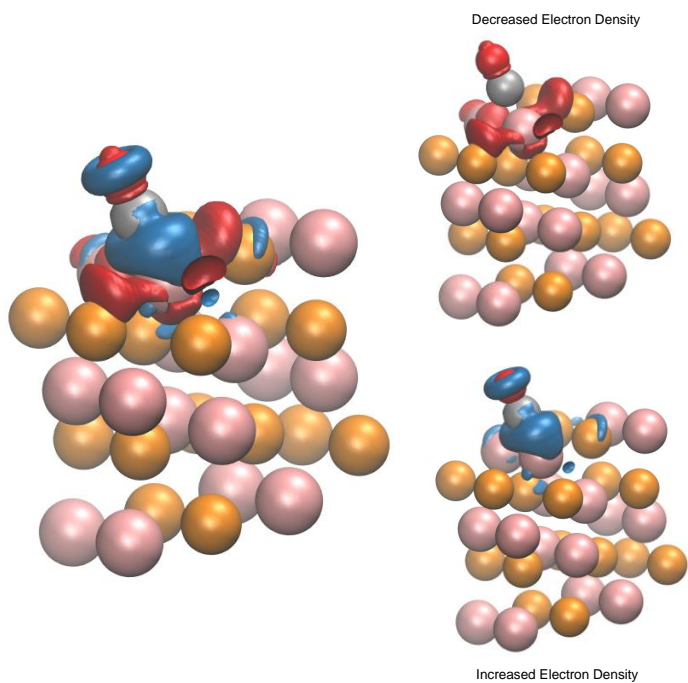
Figure S3. Panel (a) shows CO bound to a phosphorus site on the CoP surface. **Panel (b)** shows CO bound to a metallic Co site on the same CoP surface.

Charge density differences are defined so that:

$$\Delta\rho = \rho_{surf+ads} - \rho_{ads} - \rho_{surf}$$

where ρ_{ads} is the charge density of the gas phase adsorbate, ρ_{surf} the density of the pristine slab, and $\rho_{surf+ads}$ the density of the adsorbed system. Therefore, $\Delta\rho$ represents the charge transfer between the adsorbate and slab. In these calculations, the full system is fully relaxed, and a single point charge density calculation is then calculated for each density component. Red volumes represent regions of decreased electron density, while blue volumes represent regions of increased electron density. All isosurfaces are visualized in VMD and taken at +/- 0.001 isovalues (e Bohr^{-1}). For CO bound to metallic sites, significant stabilization is seen in comparison to CO bound to P-sites. This may be attributed to CO back-bonding.

Table S1. Complete Product Distribution for All Tested Catalysts

Material	Morphology	Potential (V vs. RHE)	Current Density (mA/cm²)	H_2 FE[1] (%)	CO FE[1] (%)	CH_4 FE[1] (%)	$HCOO^-$ FE[1] (%)	CA or CP[2]
MoP	Thin film	-0.39	-0.6	104	0	0	0	CA
		-0.47	-1.9	129	0	0	0	CA
		-0.50	-3.4	96	0	0	0	CA
		-0.54	-5.1	110	0	0	0	CA
		-0.57	-5.0	103	0	0	0	CP
		-0.59	-14.4	94	0	0	0	CA
CoP	Thin film	-0.29	-0.4	104	0	0	0	CA
		-0.39	-0.7	110	0	0	0	CA
		-0.48	-1.2	102	0	0	0	CA
		-0.57	-1.9	110	0	0	0	CA
		-0.61	-5.0	92	0	0	0	CP
		-0.65	-4.0	103	0	0	0	CA
		-0.67	-6.2	104	0	0	0	CA
Ni_xP	Thin film	-0.40	-0.1	101	0	Trace	0	CA
		-0.50	-0.2	123	Trace	Trace	0	CA
		-0.59	-0.6	107	0	0	0	CA
		-0.68	-1.3	94	0	0	0	CA
		-0.75	-3.6	84	Trace	0	0	CA
		-0.78	-9.0	105	Trace	0	0	CA
MoS_2	Thin film	-0.53	-0.7	100	0	0	0	CA
		-0.62	-1.9	95	0	0	0	CA
		-0.69	-4.7	112	0	0	0	CA
		-0.74	-5.0	90	0	Trace	Trace	CP
		-0.74	-10.0	99	0	0	0	CA
		-0.75	-14.6	113	0	0	0	CA
$Ni-MoS_x$	Thin film	-0.50	-0.4	98	0	0	0	CA
		-0.59	-1.3	101	0	0	0	CA
		-0.67	-3.4	92	0	0	0	CA
		-0.71	-9.0	94	0	0	0	CA

		-0.75	-14.8	95	0	0	0	CA
		-0.80	-5.0	97	0	Trace	Trace	CP
Co-MoS$_x$	Thin film	-0.40	-0.3	109	0	0	0	CA
		-0.49	-0.8	88	0	0	0	CA
		-0.59	-1.9	87	0	0	0	CA
		-0.66	-4.0	114	0	0	0	CA
		-0.73	-8.0	108	0	0	0	CA
Fe-MoS$_x$	Thin film	-0.60	-0.6	95	0	0	0	CA
		-0.68	-1.8	122	0	0	0	CA
		-0.75	-4.9	117	0	0	0	CA
		-0.79	-11.9	89	0	0	0	CA
SnS	Thin Film	-0.8	-0.6	78	1.4	0	0	CA
		-1.0	-1.3	71	3.4	0	0	CA
MoP	Nanoparticles	-0.7	-2.9	89	Trace	0	0	CA
		-0.9	-4.0	76	Trace	Trace	Trace	CA
		-1.0	-15.7	90	Trace	Trace	Trace	CA
Ni$_2$P	Nanoparticles	-0.7	-9.7	92	0	0	0	CA
		-0.85	-12.2	85	0	0	0	CA
		-0.90	-13.2	92	0	0	0	CA
CoP	Nanoparticles	-0.69	-12.0	95	0	Trace	0	CA
		-0.89	-19.6	80	0	0	0	CA
		-0.92	-19.5	91	0	Trace	0	CA
WP	Nanoparticles	-0.85	-6.2	92	Trace	Trace	0	CA
		-1.2	-15.2	91	Trace	Trace	0	CA
IrP	Nanoparticles	-0.9	-11.9	99	0	0	0	CA
RhP	Nanoparticles	-0.9	-11.4	115	0	Trace	0	CA

1. FE refers to Faradaic efficiency.
2. CA refers to chronoamperometery while CP refers to chronopotentiometry

Figure Data
Figure 1

Material	Morphology	Potential (V vs. RHE)	H$_2$ FE (%)
MoP	Thin film	-0.39	104
		-0.47	129
		-0.50	96
		-0.54	110
		-0.57	103
		-0.59	94
CoP	Thin film	-0.29	104
		-0.39	110
		-0.48	102
		-0.57	110
		-0.61	92
		-0.65	103
		-0.67	104
Ni$_x$P	Thin film	-0.40	101
		-0.50	123
		-0.59	107
		-0.68	94
		-0.75	84
		-0.78	105
MoS$_2$	Thin film	-0.53	100
		-0.62	95
		-0.69	112
		-0.74	99
		-0.74	90
		-0.75	113
Ni-MoS$_x$	Thin film	-0.50	98
		-0.59	102
		-0.67	92
		-0.71	94
		-0.75	95

		-0.80	97
Co-MoS$_x$	Thin film	-0.40	109
		-0.49	88
		-0.59	87
		-0.66	114
		-0.73	108
Fe-MoS$_x$	Thin film	-0.60	95
		-0.68	122
		-0.75	117
		-0.79	89
MoP	Nanoparticles	-0.70	89
		-0.90	76
		-1.00	90
Ni$_2$P	Nanoparticles	-0.70	92
		-0.85	85
		-0.90	92
CoP	Nanoparticles	-0.69	95
		-0.89	80
		-0.92	91
WP	Nanoparticles	-0.85	92
		-1.20	91
IrP	Nanoparticles	-0.90	99
RhP	Nanoparticles	-0.90	115
SnS	Thin Film	-0.80	78
		-1.00	71

Figure 2

Material	E vs. RHE (V)	E vs. SHE (V)	Current Density (mA/cm^2)
CoP thin film in CO$_2$, KHCO$_3$	-0.289	-0.690	-0.45
	-0.386	-0.787	-0.75
	-0.479	-0.880	-1.30
	-0.568	-0.969	-2.38
	-0.647	-1.049	-4.33
	-0.689	-1.090	-5.35
CoP thin film in Ar, KHCO$_3$	-0.259	-0.790	-0.44
	-0.350	-0.881	-1.34
	-0.432	-0.962	-3.18
	-0.499	-1.030	-6.75
	-0.522	-1.053	-15.94
MoS$_2$ thin film in CO$_2$, KHCO$_3$	-0.534	-0.935	-0.88
	-0.625	-1.026	-1.70
	-0.701	-1.102	-3.75
	-0.757	-1.158	-7.42
	-0.770	-1.171	-11.55
	-0.819	-1.220	-14.77
MoS$_2$ thin film in Ar, KHCO$_3$	-0.406	-0.937	-0.56
	-0.491	-1.022	-1.46
	-0.572	-1.103	-2.69
	-0.632	-1.163	-5.16
	-0.680	-1.211	-8.65
	-0.699	-1.230	-15.91
CoP thin film in H$_2$, H$_2$SO$_4$	-0.112	-0.112	-0.21
	-0.115	-0.115	-0.24
	-0.118	-0.118	-0.27
	-0.121	-0.121	-0.31
	-0.124	-0.124	-0.35
	-0.127	-0.127	-0.39
	-0.130	-0.130	-0.45
	-0.133	-0.133	-0.51
	-0.136	-0.136	-0.57
	-0.139	-0.139	-0.65
	-0.142	-0.142	-0.74
	-0.145	-0.145	-0.83
	-0.149	-0.149	-0.95
	-0.151	-0.151	-1.07
	-0.154	-0.154	-1.21
	-0.158	-0.158	-1.38
	-0.161	-0.161	-1.57
	-0.164	-0.164	-1.76

	-0.167	-0.167	-1.98
	-0.170	-0.170	-2.22
	-0.173	-0.173	-2.48
	-0.176	-0.176	-2.78
	-0.178	-0.178	-3.10
	-0.181	-0.181	-3.45
	-0.184	-0.184	-3.85
	-0.187	-0.187	-4.28
	-0.190	-0.190	-4.75
	-0.193	-0.193	-5.26
	-0.195	-0.195	-5.82
	-0.198	-0.198	-6.42
	-0.201	-0.201	-7.08
	-0.203	-0.203	-7.79
	-0.206	-0.206	-8.53
	-0.209	-0.209	-9.34
	-0.211	-0.211	-10.23
MoS_2 thin film in H_2, H_2SO_4	-0.203	-0.203	-0.20
	-0.204	-0.204	-0.21
	-0.205	-0.205	-0.22
	-0.206	-0.206	-0.23
	-0.207	-0.207	-0.24
	-0.208	-0.208	-0.25
	-0.208	-0.208	-0.26
	-0.210	-0.210	-0.27
	-0.211	-0.211	-0.28
	-0.211	-0.211	-0.29
	-0.212	-0.212	-0.30
	-0.214	-0.214	-0.31
	-0.215	-0.215	-0.33
	-0.216	-0.216	-0.34
	-0.217	-0.217	-0.35
	-0.217	-0.217	-0.37
	-0.218	-0.218	-0.38
	-0.219	-0.219	-0.40
	-0.220	-0.220	-0.42
	-0.221	-0.221	-0.43
	-0.222	-0.222	-0.45
	-0.223	-0.223	-0.47
	-0.224	-0.224	-0.49
	-0.225	-0.225	-0.51
	-0.226	-0.226	-0.53
	-0.227	-0.227	-0.55
	-0.228	-0.228	-0.57
	-0.229	-0.229	-0.60

	-0.230	-0.230	-0.62
	-0.231	-0.231	-0.64
	-0.232	-0.232	-0.67
	-0.233	-0.233	-0.70
	-0.234	-0.234	-0.72
	-0.234	-0.234	-0.76
	-0.236	-0.236	-0.78
	-0.236	-0.236	-0.81
	-0.237	-0.237	-0.85
	-0.238	-0.238	-0.88
	-0.239	-0.239	-0.91
	-0.240	-0.240	-0.95
	-0.241	-0.241	-0.98
	-0.242	-0.242	-1.01
	-0.243	-0.243	-1.05
	-0.244	-0.244	-1.09
	-0.245	-0.245	-1.13
	-0.246	-0.246	-1.17
	-0.247	-0.247	-1.21
	-0.248	-0.248	-1.25
	-0.248	-0.248	-1.30
	-0.250	-0.250	-1.34
	-0.250	-0.250	-1.38
	-0.251	-0.251	-1.43
	-0.252	-0.252	-1.48
	-0.253	-0.253	-1.52
	-0.254	-0.254	-1.58
	-0.255	-0.255	-1.63
	-0.256	-0.256	-1.67
	-0.257	-0.257	-1.73
	-0.257	-0.257	-1.78
	-0.258	-0.258	-1.84
	-0.259	-0.259	-1.90
	-0.260	-0.260	-1.95
	-0.261	-0.261	-2.00
	-0.262	-0.262	-2.07
	-0.263	-0.263	-2.13
	-0.264	-0.264	-2.18
	-0.264	-0.264	-2.25
	-0.265	-0.265	-2.31
	-0.266	-0.266	-2.37
	-0.267	-0.267	-2.44
	-0.268	-0.268	-2.51
	-0.269	-0.269	-2.57
	-0.270	-0.270	-2.64

	-0.271	-0.271	-2.71
	-0.271	-0.271	-2.78
	-0.272	-0.272	-2.85
	-0.273	-0.273	-2.92
	-0.274	-0.274	-2.99
	-0.275	-0.275	-3.07
	-0.276	-0.276	-3.14
	-0.277	-0.277	-3.21
	-0.277	-0.277	-3.30
	-0.278	-0.278	-3.37
	-0.279	-0.279	-3.44
	-0.280	-0.280	-3.53
	-0.281	-0.281	-3.61
	-0.282	-0.282	-3.68
	-0.282	-0.282	-3.77
	-0.283	-0.283	-3.86
	-0.284	-0.284	-3.93
	-0.285	-0.285	-4.02
	-0.286	-0.286	-4.11
	-0.286	-0.286	-4.19
	-0.287	-0.287	-4.28
	-0.288	-0.288	-4.37
	-0.289	-0.289	-4.45
	-0.290	-0.290	-4.55
	-0.291	-0.291	-4.64
	-0.291	-0.291	-4.72
	-0.292	-0.292	-4.82
	-0.293	-0.293	-4.92
	-0.294	-0.294	-5.00
	-0.294	-0.294	-5.10
	-0.295	-0.295	-5.20
	-0.296	-0.296	-5.29
	-0.297	-0.297	-5.39
	-0.298	-0.298	-5.49
	-0.299	-0.299	-5.58
	-0.299	-0.299	-5.69
	-0.300	-0.300	-5.79
	-0.301	-0.301	-5.88
	-0.302	-0.302	-5.99
	-0.302	-0.302	-6.09
	-0.304	-0.304	-6.19
	-0.304	-0.304	-6.30
	-0.305	-0.305	-6.41
	-0.306	-0.306	-6.50
	-0.307	-0.307	-6.61

-0.308	-0.308	-6.72
-0.308	-0.308	-6.82
-0.309	-0.309	-6.93
-0.310	-0.310	-7.05
-0.311	-0.311	-7.14
-0.311	-0.311	-7.26
-0.312	-0.312	-7.37
-0.313	-0.313	-7.47
-0.314	-0.314	-7.59
-0.314	-0.314	-7.71
-0.315	-0.315	-7.81
-0.316	-0.316	-7.93
-0.317	-0.317	-8.05
-0.318	-0.318	-8.15
-0.318	-0.318	-8.27
-0.319	-0.319	-8.40
-0.320	-0.320	-8.50
-0.320	-0.320	-8.62
-0.321	-0.321	-8.75
-0.322	-0.322	-8.85
-0.323	-0.323	-8.97
-0.324	-0.324	-9.10
-0.324	-0.324	-9.21
-0.325	-0.325	-9.33
-0.326	-0.326	-9.46
-0.327	-0.327	-9.57
-0.327	-0.327	-9.70
-0.328	-0.328	-9.83
-0.329	-0.329	-9.94
-0.330	-0.330	-10.06
-0.330	-0.330	-10.20

Figure 3a

E Phosphides	E_{CO}	E_{CHO}
MoP	0.369	-1.05
FeP	-1.193	-0.845
Fe_2P	-1.653	-1.695
CoP	-1.86	-1.748
Co_2P	-1.634	-1.084
Ni_2P	-1.331	-1.023
$Fe_{0.5}Co_{0.5}P$	-1.801	-1.683

E Sulfides	E_{CO}	E_{CHO}
MoS_2	-0.37	-0.85
Ni-MoS_2	-0.67	-1.1

211 Metals	E_{CO}	E_{CHO}
Pt	-1.77	-1.55
Pd	-1.67	-1.21
Cu	-0.75	-0.55
Au	-0.31	-0.35
Ag	-0.22	0.009
Ir	-2.19	-1.93
Rh	-1.81	-1.61
Ni	-1.87	-1.56

111 Metals	E_{CO}	E_{CHO}
Pt	-1.47	-1.31
Pd	-1.77	-1.2
Cu	-0.48	-0.09
Au	-0.009	-0.17
Ag	-0.08	0.21
Rh	-1.68	-1.33
Ni	-1.88	-1.33
Ir	-1.47	-1.14

Figure 3b

	E_{CO}	$U_{L\ HER}$
MoP	0.369	-0.166
FeP	-1.193	-0.133
Fe_2P	-1.653	-0.123

CoP	-1.86	-0.085
Co_2P	-1.634	-0.212
Ni_2P	-1.331	-0.138
$Fe_{0.5}Co_{0.5}P$	-1.801	-0.029
MoS_2	-0.37	-0.11
Ni-MoS_2	-0.67	-0.1

	E_{CO}	$U_{L\ CO2R}$
MoP	0.369	-0.967
FeP	-1.193	-0.861
Fe_2P	-1.653	-1.369
CoP	-1.86	-0.645
Co_2P	-1.634	-1.078
Ni_2P	-1.331	-0.836
$Fe_{0.5}Co_{0.5}P$	-1.801	-0.604
MoS_2	-0.37	-0.62
Ni-MoS_2	-0.67	-0.28

Figure 4d

Ni-MoS$_2$		MoS$_2$	
Work Function (eV)	G$_a$ (eV)	Work Function (eV)	G$_a$ (eV)
0	-0.8	0	-0.04
4	1.09	4	1.35
8	2.98	8	2.75

The values in this table are derived using methods detailed in work by Chan et al.[10] This process involves performing a nudged elastic band calculation to define the barrier between an initial and final state. Upon convergence, the energy, work function, and charge of the initial, transition, and final states are calculated. Using a simple capacitor model of the interface and these calculated quantities, you can relate the energy of the transition state to potential via a linear relationship; this method is implemented to correct for inherent errors introduced by using finite-sized charged cells in DFT calculations.

Recall that the work function is related to the absolute potential vs. the standard hydrogen electrode where 4.4 eV is the experimentally determined value of Φ_{SHE}.

$$U_{SHE} = \frac{\Phi - 4.4 \text{ eV}}{e}$$

After determining the linear relationship between potential and the activation energy, G$_a$, we can find the barrier at 0 V on an RHE scale. We assume a pH of 7 and evaluate the relationship between activation energy and potential at the appropriate work function (corresponds to a $\Phi = 4.4 \ eV - 0.059 \ eV * 7 \approx 4.0 \ eV$).

$$G_{a\,MoS2} = 0.47 * \Phi - 0.8 \text{ eV}$$

$$G_{a\,NiMoS2} = 0.35 * \Phi - 0.04 \text{ eV}$$

Therefore:

$$G_{a\,MoS2}(0 \text{ V vs RHE, pH 7}) = 0.47 * 4.0 \text{ eV} - 0.8 \text{ eV} = 1.09 \text{ eV}$$

The dependence of the barriers on applied potential are determined using the calculated transfer coefficients (0.47 and 0.35 for MoS$_2$ and NiMoS$_2$ respectively). These transfer coefficients are calculated from the charge of the transition state compared to the initial state. We typically assume a barrier of 0.75 eV as a threshold for facile kinetics. Since the activation energy scales with electrons transferred, potential, and the transfer coefficient, we can find the barrier at a given applied potential below 0 V vs. RHE. For example, if we want to determine the potential which must be applied to achieve facile kinetics:

$$G_{a\,MoS2} = 1.09 \text{ eV} + (0.47 * U_{RHE})$$

$$G_{a\,Ni-MoS2} = 1.35 \text{ eV} + (0.35 * U_{RHE})$$

We find in the case of MoS$_2$, -0.72 V corresponds to a G$_a$ = 0.75 eV.

Figure 4e

FCC (211)	
E$_{CO}$ (eV)	G$_a$ (eV)
-0.22	0.86
-0.29	0.95
-0.81	0.97
-1.75	1.56
-1.79	1.58
-1.87	1.73
FCC (111)	
-0.1	1.05
-0.03	0.98
-0.5	1.34
-1.49	1.89
-1.88	2.1
MoS$_2$	
-0.37	1.09
Ni-MoS$_2$	
-0.67	1.35

References

(1).   Hellstern, T. R.; Benck, J. D.; Kibsgaard, J.; Hahn, C.; Jaramillo, T. F. Engineering Cobalt Phosphide (CoP) Thin Film Catalysts for Enhanced Hydrogen Evolution Activity on Silicon Photocathodes. *Adv. Energy Mater.* **2016,** *6*, 1501758.

(2).   Benck, J. D.; Lee, S. C.; Fong, K. D.; Kibsgaard, J.; Sinclair, R.; Jaramillo, T. F. Designing Active and Stable Silicon Photocathodes for Solar Hydrogen Production Using Molybdenum Sulfide Nanomaterials. *Adv. Energy Mater.* **2014,** *4*, 1400739.

(3).   Kuhl, K.; Cave, E.; Abram, D.; Jaramillo, T. New Insights into the Electrochemical Reduction of Carbon Dioxide on Metallic Copper Surfaces. *Energy Environ. Sci.* **2012,** *5*, 7050-7059.

(4).   Henkes, A.; Schaak, R. Trioctylphosphine: A General Phosphorus Source for the Low-Temperature Conversion of Metals into Metal Phosphides. *Chem. Mater.* **2007,** *19*, 4234-4242.

(5).   Callejas, J.; Read, C.; Roske, C.; Lewis, N.; Schaak, R. Synthesis, Characterization, and Properties of Metal Phosphide Catalysts for the Hydrogen-Evolution Reaction. *Chem. Mater.* **2016,** *28*, 6017-6044.

(6).   Popczun, E.; McKone, J.; Read, C.; Biacchi, A.; Wiltrout, A.; Lewis, N.; Schaak, R. Nanostructured Nickel Phosphide as an Electrocatalyst for the Hydrogen Evolution Reaction. *J. Am. Chem. Soc.* **2013,** *135*, 9267-9270.

(7).   Antunez, P. D.; Torelli, D. A.; Yang, F.; Rabuffetti, F. A.; Lewis, N. S.; Brutchey, R. L. Low Temperature Solution-Phase Deposition of SnS Thin Films. *Chem. Mater.* **2014,** *26*, 5444-5446.

(8).   Webber, D. H.; Brutchey, R. L. Alkahest for V_2VI_3 Chalcogenides: Dissolution of Nine Bulk Semiconductors in a Diamine-Dithiol Solvent Mixture. *J. Am. Chem. Soc.* **2013,** *135*, 15722-15725.

(9).   Henkelman, G.; Uberuaga, B.; Jonsson, H. A Climbing Image Nudged Elastic Band Method for Finding Saddle Points and Minimum Energy Paths. *J. Chem. Phys.* **2000,** *113*, 9901-9904.

(10).   Chan, K.; Nørskov, J. K. Electrochemical Barriers Made Simple. *J. Phys. Chem. Lett.* **2015,** *6*, 2663-2668.

(11).   Chan, K.; Nørskov, J. K. Potential Dependence of Electrochemical Barriers from ab Initio Calculations. *J. Phys. Chem. Lett.* **2016,** *7*, 1686-1690.

(12).   Henkelman, G.; Arnaldsson, A.; Jonsson, H. A Fast and Robust Algorithm for Bader Decomposition of Charge Density. *Comput. Mater. Sci.* **2006,** *36*, 354-360.

(13).   Kibsgaard, J.; Tsai, C.; Chan, K.; Benck, J.; Nørskov, J.; Abild-Pedersen, F.; Jaramillo, T. Designing an Improved Transition Metal Phosphide Catalyst for Hydrogen Evolution Using Experimental and Theoretical Trends. *Energy Environ. Sci.* **2015,** *8*, 3022-3029.

(14).   Hong, X.; Chan, K.; Tsai, C.; Nørskov, J. How Doped MoS_2 Breaks Transition-Metal Scaling Relations for CO_2 Electrochemical Reduction. *ACS Catal.* **2016,** *6*, 4428-4437.

(15).   Liu, X.; Xiao, J.; Peng, H.; Hong, X.; Chan, K.; Nørskov, J. K. Understanding Trends in Electrochemical Carbon Dioxide Reduction Rates. *Nat. Commun.* **2017,** *8*, 15438.